Correlation effects of a phase-diffusing field on two-photon absorption

D. S. Elliott,* M. W. Hamilton, K. Arnett, and S. J. Smith†
Joint Institute for Laboratory Astrophysics, University of Colorado and National Bureau of Standards, Boulder, Colorado 80309
(Received 7 February 1985)

Experimental evidence of field-correlation effects on weak-field two-photon absorption in atomic sodium is presented. In the case of a nearly Lorentzian laser power spectrum the absorption profile has four times the spectral width of the exciting field, in agreement with predictions by Mollow. The measurement is carried out with counterpropagating laser beams to cancel Doppler broadening. The width of the two-photon absorption spectrum is decreased by partially decorrelating the counterpropagating laser beams. Increasing the correlation time of the frequency fluctuations, resulting in a nearly Gaussian laser power spectrum, has also been observed to decrease the width of the absorption spectrum. An extension of the time-dependent second-order perturbation theory to these additional cases yields good agreement.

I. INTRODUCTION

Laser bandwidth effects in nonlinear optics have received much theoretical attention over the past twenty years, but very little quantitative experimental work has been performed to serve as a comparison. We recently reported[1,2] an experiment which provided information on the effect of a laser field undergoing random frequency fluctuations (resulting in a nearly Lorentzian laser power spectrum) on an unsaturated two-photon absorption process. Here we give a more complete account on this experiment including extensions to non-Lorentzian power spectra and to field-correlation effects.

The first theoretical treatment of the frequency response of an atom for a two-photon process was presented by Mollow[3] who showed that the weak-field absorption spectrum is simply the Fourier transform of a second-order correlation function of the electric field. He then applied this result in the special cases of (1) the "chaotic" field, by which he meant that the field amplitude undergoes random fluctuations and frequency is fixed, and (2) a phase-diffusing field, for which the frequency undergoes random fluctuations and amplitude is fixed. Specifically, when the applied field had a Lorentzian power spectrum of width b, the absorption spectrum was calculated to be Lorentzian of width $2b$ for the chaotic field, and of width $4b$ for the phase-diffusing field. The difference between the predictions for these two laser fields is dramatic and is one example of the incompleteness of the information about the field provided by the laser power spectrum. The laser power spectrum defines only the lowest-order correlation function of the electric field, whereas the second-order correlation function determines the response of the atom for a two-photon absorption process.

Agarwal[4] extended Mollow's work to the case of n-photon absorption, and, for a Lorentzian laser power spectrum of width b, showed that the absorption width equals nb for the chaotic field and n^2b for the phase-diffusing field.

Alber and Zoller[5] considered the problem of two-photon absorption using a density-matrix formulation, yielding results valid for strong fields as well. In the weak-field limit, their results reduce to those reported by Mollow.

Similar results are obtained when the problem of n-photon resonant, $(n+1)$-photon ionization is considered. In the work of Zoller and Lambropoulos[6] and Yeh and Eberly[7] a formalism based on the equations of motion of the density matrix was used, also yielding results valid for higher intensities. In general, this ionization rate is different from two-photon absorption, but in the limit of fast fluctuations, the bound-bound transition and the ionization step decorrelate, and the absorption spectrum becomes the same for the two processes.[6,7]

As the experimental work reported here is done with weak fields, we use Mollow's perturbation methods when extending the theory to conform to the field correlations of our experiment. This is presented in Sec. II. The experiment is described in Sec. III and the results are presented in Sec. IV.

II. THEORY

The laser field which we produce experimentally realizes the properties of the phase-diffusion model. This field is characterized by

$$E(t)=E_0e^{-i[\omega_0t+\phi(t)]}, \tag{1}$$

where E_0 and ω_0 are the constant amplitude and the mean frequency of the field, respectively. The phase $\phi(t)$ is a random Gaussian variable related to a random Gaussian frequency $\omega(t)$ by $\omega(t)=d\phi(t)/dt$. The frequency is stationary in a statistical sense. The correlation function of the frequency is given by

$$\langle\omega(t)\omega(t+\tau)\rangle=b\beta e^{-\beta|\tau|}, \tag{2}$$

where b is the spectral density of the frequency fluctuations, and $1/\beta$ is the correlation time of the fluctuations.

The angular brackets denote an ensemble-averaging procedure. The product $b\beta$ can be identified as the average of the square of the frequency fluctuation. These two parameters completely determine the statistical properties of the laser field and, as will be seen later, correspond to experimentally variable features of the noise power spectrum applied to the laser field.

The power spectrum of the laser field is given by

$$P(\Delta\omega)=|E_0|^2\int_0^\infty d\tau\cos(\Delta\omega\tau)\times\exp\left[-b\tau+\frac{1}{\beta}(e^{-\beta\tau}-1)\right]. \quad (3)$$

Limiting cases have been discussed in some detail by Elliott *et al.*[8] When the fluctuations of the frequency are fast, $\beta\gg b$, the laser power spectrum tends to a Lorentzian function of half-width at half maximum (HWHM) b near line center, but falls off more rapidly than Lorentzian in the far wings. As the correlation time β^{-1} goes to zero, the correlation function of the frequency, Eq. (2), becomes a δ function, and the power spectrum becomes exactly Lorentzian. This is the original phase-diffusion model which was employed by Mollow in his treatment of the two-photon absorption problem.

For very slow fluctuations, $\beta\ll b$, the power spectrum is similar to a Gaussian function, with HWHM $[(2\ln 2)b\beta]^{1/2}$. The frequency has a long "memory" in this case, remaining essentially constant for a time $1/\beta$. This, strictly speaking, is not diffusion of the phase, but is generally considered to be an extension of the phase-diffusion model.

Using a second-order time-dependent perturbation method, Mollow derived the relation between the two-photon absorption profile, W_2, and the second-order correlation function of the applied fields, $G^{(2)}$:

$$W_2=2|g(\omega_0)|^2\int_{-\infty}^{\infty}dt\,e^{2i\omega_f t-\kappa_f|t|}G^{(2)}(-t,-t;t,t)\,. \quad (4)$$

The energy and full width at half maximum (FWHM) of the excited state are given by $\hbar\omega_f$ and κ_f, respectively, and $g(\omega_0)$ is the transition moment of the two-photon transition whose explicit form does not affect the discussion at hand. The correlation function $G^{(2)}$ for a single-mode field is defined as

$$G^{(2)}(t_1',t_2';t_1,t_2)=\langle E^*(t_1')E^*(t_2')E(t_1)E(t_2)\rangle\,.$$

For a phase-diffusing field with δ-correlated frequency fluctuations with a (Lorentzian) spectral half-width of b, Mollow showed that the absorption spectrum is a Lorentzian with half-width $\sim 4b$:

$$W_2=I^2|g(\omega_0)|^2\frac{2(4b+\frac{1}{2}\kappa_f)}{(4b+\frac{1}{2}\kappa_f)^2+(2\omega_0-\omega_f)^2}\,. \quad (5)$$

Using the same model for the laser field, Agarwal generalized this result to an n-photon absorption process, showing that the width of the absorption profile increases as n^2.

Mollow's result can be extended to include two modifications relevant to our experiment. First, we include the effect of having frequency fluctuations with a finite correlation time.[2] This is done by using the correlation function of the frequency fluctuations as given by Eq. (2), rather than the δ-correlated fluctuations used by Mollow. The second feature which we include is to replace the single field used in Mollow's treatment by the sum of two fields $E_1(t)+E_2(t)$, where the second field is the same as the first field at an earlier time, $E_2(t)=E_1(t-\tau_D)$. In the experiment, this corresponds to the use of counterpropagating laser beams which are necessary for Doppler-free two-photon spectroscopy in a vapor, and τ_D is the round-trip time necessary for the light to travel from the interaction region to a reflector and back to the interaction region.

Incorporation of the nonzero correlation time, β^{-1}, and the time delay, τ_D, into the electric field yields a second-order correlation function of the form

$$G^{(2)}(-t,-t;t,t)=e^{-i4\omega_0 t}4\exp\left[2b\left[\tau_D+\frac{1}{\beta}(e^{-\beta\tau_D}-1)\right]-2b\left[2|t|+\frac{1}{\beta}(e^{-2\beta|t|}-1)\right]-b\left[|2t-\tau_D|+\frac{1}{\beta}(e^{-\beta|2t-\tau_D|}-1)\right]-b\left[|2t+\tau_D|+\frac{1}{\beta}(e^{-\beta|2t+\tau_D|}-1)\right]\right]. \quad (6)$$

The Fourier transform of this function yields the absorption spectrum. It is instructive to examine this absorption spectrum for different values of the delay time and correlation time. Neglecting the effect of spontaneous decay of the excited state, we see that the absorption spectrum is Gaussian (Lorentzian) if the laser power spectrum is Gaussian (Lorentzian). If the laser power spectrum is intermediate between these two shapes ($\beta\sim b$), the absorption spectrum is similar to, but possesses a somewhat more Gaussian nature than, the laser power spectrum.

The effect of a nonzero delay is to provide an opportunity for the two fields to decorrelate, resulting in a decrease in the width of the absorption spectrum. The ratio of the absorption width $(\Delta\omega)_{\text{abs}}$ to the laser linewidth $(\Delta\omega)_L$ is given in Table I. The factor of 4 given by Mollow is found for the near-Lorentzian case ($\beta\gg b$) with no delay ($\tau_D\ll 1/2b$). If the two fields are allowed to completely decorrelate, the width of the absorption spectrum is halved. The delay time necessary for decorrelation scales as the inverse of the laser bandwidth in this case. This field decorrelation introduced by delaying one laser beam is equivalent to the use of two independently generated laser fields, each with the same near-Lorentzian characteristics.

When the laser line shape is nearly Gaussian, the absorption linewidth is simply twice the laser width for the completely correlated case. This result is much more intuitively obvious than that for the Lorentzian line shape.

TABLE I. Limiting values of absorption-width $(\Delta\omega)_{abs}$ to laser-profile-width $(\Delta\omega)_L$ ratios.

$\beta \gg b$ (Lorentzian)	$(\Delta\omega)_{abs}/(\Delta\omega)_L$	$\beta \ll b$ (Gaussian)	$(\Delta\omega)_{abs}/(\Delta\omega)_L$
$\tau_D \ll \frac{1}{2b}$	4	$\tau_D \ll \frac{1}{\beta}$	2
$\tau_D \gg \frac{1}{2b}$	2	$\tau_D \gg \frac{1}{\beta}$	$\sqrt{2}$

Since the fluctuations are rather slow in this case, the power spectrum of the laser is the same as the probability distribution of the field frequency. Absorption can take place whenever the sum of the field frequencies $\omega_1+\omega_2$ is equal to the transition frequency ω_f. The width of the probability distribution of the sum of two Gaussian variables (having the same width, $\Delta\omega$) is then $2\Delta\omega$ if the variables are completely correlated. A delay time greater than the correlation time of the frequency fluctuations β^{-1} is necessary to decorrelate the fields for the Gaussian power spectrum, reducing the absorption width by the factor $\sqrt{2}$. This width is the width of the probability distribution of the sum of two uncorrelated Gaussian variables.

In addition to the limiting cases discussed above, the Fourier transform of Eq. (6) can be evaluated numerically to determine the absorption spectrum for arbitrary correlation time and delay time. This procedure is used to calculate the widths and relative heights of the absorption spectra for comparison with the experimental results.

III. EXPERIMENTAL METHOD

Some aspects of the technique for superposing frequency fluctuations onto the laser beam have been discussed in previous reports.[8,9] We present here a complete description of that technique. The method uses a statistically characterized random voltage to modulate the laser frequency and phase with wide-bandwidth acousto-optic and electro-optic modulators. Because of technical limitations described below, the frequency-modulation technique is preferred for the low-frequency modulation, while the phase modulation has advantages in the high-frequency range.

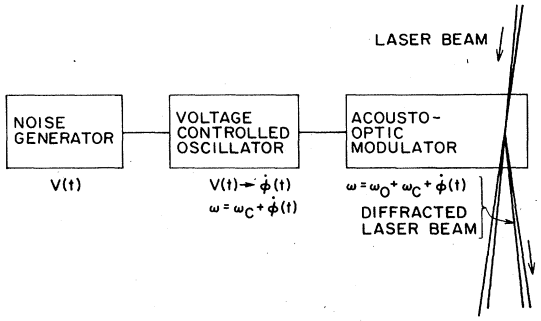

FIG. 1. Simplified diagram of the frequency-modulation apparatus. The voltage-controlled oscillator transforms the fluctuating voltage $V(t)$ into a fluctuating frequency $\dot{\phi}(t)$. The acousto-optic modulator adds the fluctuating frequency $\dot{\phi}(t)$ and the carrier frequency ω_c to the frequency of the incident laser field ω_0 so that the frequency of the diffracted laser beam is a fluctuating variable.

The basic components of the frequency-modulation process consist of a noise voltage source, a voltage controlled oscillator, and an acousto-optic modulator (see Fig. 1). The random (Gaussian) voltage, on which the laser bandwidth synthesis is based, is derived from a noise source consisting of an avalanche-mode diode. The properties of this random voltage will be discussed in more detail later in this section. The random voltage is used to modulate the frequency of the constant-amplitude rf signal produced by the voltage-controlled oscillator. The final step of this frequency-modulation process is to transfer these fluctuations to the laser field. This is accomplished by driving the acousto-optic modulator with the modulated rf signal, which adds the frequency of the driving signal to the frequency of the laser field.

Since the correlation function and the power spectrum of the laser frequency fluctuations are related through the Fourier transform, the spectral density of the frequency fluctuations must follow a Lorentzian function

$$P_{FM}(\omega)=b[1+(\omega/\beta)^2]^{-1} \tag{7}$$

in order to realize the correlation function, Eq. (2). This was achieved by constructing simple shaping circuits consisting of 50-Ω transmission lines, external capacitors, and wide-band single-stage amplifiers used as buffers (for isolation). In all cases, the output noise level was at least 13 dB lower than the output capability of the amplifiers, ensuring that the random voltage was distorted (clipped) less than 0.001% of the time. The spectral density of the noise, b, was controlled by amplification or attenuation of the random-voltage signal, and the correlation time, β^{-1}, was controlled by changing the filter which controls the Lorentzian power spectrum. The noise power spectrum used in the experiment was shaped to within 1 dB/MHz of that given by Eq. (7). There are, however, limitations to the use of an acousto-optic modulator. These are related to (1) the frequency dependence of the angle at which the light is diffracted by the modulator, (2) the finite velocity of sound in the acousto-optic crystal, and (3) the finite bandwidth of the modulator.

The operation of an acousto-optic modulator is based on the diffraction of the laser radiation from a grating formed by an acoustic wave traveling across the crystal. The light and sound waves propagate in directions nearly perpendicular to each other. The angular deviation of the diffracted beam from the incident beam varies linearly with the frequency of the acoustic wave. If the acoustic frequency changes, as it does for the fluctuating-frequency rf signal used in this experiment, the diffraction angle changes.

To eliminate this effect, the diffracted laser beam is collimated, retroreflected using a right-angle prism and focused back into the acousto-optic modulator. On the second pass through the modulator the diffraction angle is the same as on the first pass (provided the acoustic frequency has not had sufficient time to change) and the twice-diffracted beam is antiparallel to the incident laser beam, independent of the acoustic frequency. The use of a right-angle prism allows for the spatial separation of the laser beams. This double-pass procedure has the added

benefit of doubling the magnitude of the frequency fluctuation imposed on the laser beam.

The finite velocity of the acoustic wave in the acousto-optic crystal determines the maximum rate at which the acoustic frequency can be modulated for a given size of laser beam in the crystal. For the acousto-optic modulator used in this experiment, the beam waist diameter of the laser was 30 μm. In order for the frequency of the diffracted light to be spatially uniform across the beam, the acoustic frequency should be nearly constant in the acoustic interaction region. We have chosen 6 MHz as the maximum rate at which the optical frequency is modulated. At this limit the average difference in frequency across the laser beam is about 20% of the root-mean-square frequency fluctuation. The frequency fluctuations of the acoustic wave become uncorrelated in a distance of approximately 600 μm, much larger than the size of the focused laser.

The final limitation of the acousto-optic modulator is the finite bandwidth of the modulator. As the acoustic frequency driving the modulator is changed from the center frequency, the intensity of the diffracted light decreases. This is due to a combination of processes such as a change of the Bragg angle of the modulation, a change of the acoustic field pattern in the crystal, and the frequency dependence of the impedance matching between the 50-Ω transmission line and the input circuitry of the modulator. The full width at half maximum of the modulator is in excess of 100 MHz for our model. To maintain the acoustic frequency within the flattest portion of the modulator response (50 MHz full width), the root-mean-square fluctuation of the frequency must be limited to approximately 6 MHz allowing for frequency excursions of four standard deviations. The use of the double pass through the acousto-optic modulator is beneficial here, increasing the maximum laser bandwidth for a Gaussian laser power spectrum to approximately 30 MHz.

A full schematic of the random frequency-modulation process is shown in Fig. 2. The power spectrum of the fluctuating voltage generated by the noise source is shaped according to a Lorentzian form [Eq. (7)], limited to frequencies less than 6 MHz, and amplified or attenuated as necessary. The voltage-controlled oscillator that we used operated at a frequency of $\sim$3.5 GHz and was mixed with a 3.7-GHz local oscillator signal to obtain the 200-MHz signal required by the acousto-optic modulator. Amplification of the 200-MHz fluctuating-frequency signal to a power of 1 W was necessary. Nonlinearities in the tuning curve (frequency out versus voltage in) of the voltage-controlled oscillator were measured and determined to be insignificant for this process.

The phase-modulation process was used to impose the high-frequency fluctuations onto the laser beam, in order to control the laser line shape to 1 GHz from line center. For this purpose a traveling-wave electro-optic crystal was used, to which the random voltage fluctuations were directly applied. In general, the field produced by phase modulation with a signal having a power spectrum $P_{\phi M}(\omega)$ is indistinguishable from that produced by frequency modulation using the power spectrum $P_{FM}(\omega)$ if the two power spectra are related by [10]

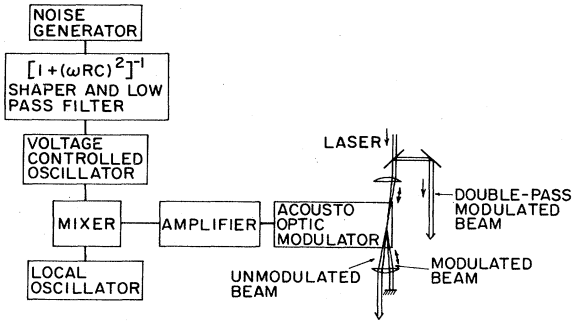

FIG. 2. Detailed diagram of the frequency-modulation apparatus used for superposing low-frequency fluctuations onto the laser frequency.

$$P_{\phi M}(\omega)=P_{FM}(\omega)\omega^{-2}\,. \tag{8}$$

Again, shaping circuits similar to those described above were used to make the noise power spectrum conform to within 1 dB/MHz of the power spectrum defined by Eqs. (7) and (8). Since $P_{FM}(\omega)$ has a finite value at low frequencies b, the power spectral density of the equivalent phase-modulation process becomes prohibitively large in this region. This defines a minimum frequency at which the phase-modulation process is practical. If 6 MHz is chosen as this minimum frequency (corresponding to the maximum frequency for the frequency-modulation process), 2 W of phase-modulating noise power are required to produce a nearly Lorentzian laser line shape with a width (FWHM) of 20 MHz. A wide-band 40-W amplifier is needed to drive the electro-optic modulator, the excess output capability being necessary to avoid clipping of the larger excursions of the random (Gaussian) driving signal. The modulator used consists of a $LiTaO_3$ crystal of dimension $0.65\times0.50\times25$ mm^3. The crystal geometry causes the modulator to behave as a plane-parallel transmission line, with a nominal characteristic impedance of 50 Ω (we measured this value to be $\sim$45 Ω using a time-domain reflectometer). Phase-modulation sidebands are easily attainable at a separation greater than 1 GHz using these modulators. Because of the power and frequency requirements necessary for driving the electro-optic modulator, two separate electro-optic modulators were used, one for intermediate frequencies (6—200 MHz) and one for high frequencies (200 MHz—1 GHz). In this way, two separate amplifiers of much more modest specifications could be used. A diagram of the phase-modulation apparatus is shown in Fig. 3. A simple cross-over network was used to separate the noise components above or below 200 MHz, and route them toward the appropriate modulator.

The power spectrum of the laser was monitored using a heterodyne technique. A component of the linewidth-broadened laser beam and a component of the unbroadened laser beam were combined on a beamsplitter and directed onto a fast photodiode operating in the avalanche regime. Since the acousto-optic modulator used in the frequency-modulation process produced a frequency offset of 200 MHz for each pass of the laser beam, the

linewidth-broadened laser differed in frequency by 400 MHz from the unmodulated laser. Thus the heterodyne signals produced by the avalanche photodiode appeared at 400 MHz. The signal was amplified (30 dB) and displayed directly on an rf spectrum analyzer. The width of the laser power spectrum was determined from a plot generated by the spectrum analyzer interfaced to an x-y recorder.

Adjustment of the relative power levels of the noise used in the frequency- and phase-modulation apparatus was necessary in order to obtain the desired laser power spectrum. Approximate matching was achieved using the design characteristics of the devices involved, but fine tuning of the noise levels while monitoring the laser power spectrum proved to be essential. In this manner, laser power spectra were matched to within 1 dB/MHz of the desired laser power spectra as determined by numerical calculations of Eq. (3). A typical laser power spectrum is shown in Fig. 4.

It is critical for these measurements that the fluctuations have a Gaussian probability distribution. This feature ensures that the even, higher-order correlation functions of the fluctuations are related to the lowest-order correlation function by the relation[11]

$$\langle \omega(t_1)\omega(t_2)\cdots\omega(t_{2n})\rangle = \sum_{\substack{\text{all}\\ \text{permutations}}} \langle \omega(t_i)\omega(t_j)\rangle\cdots\langle \omega(t_k)\omega(t_l)\rangle$$

and that the odd-order correlation functions are zero. Since the electric field and the frequency are related nonlinearly (sinusoidally), the statistical properties of the field depend on the correlation functions of the frequency to all orders. The Gaussian nature of the fluctuations must therefore be demonstrated in the laboratory.

All fluctuations in the experiment are derived from a random voltage produced by avalanche diodes. In the time domain the noise is composed of a random succession of pulses corresponding to the traversal of electrons across the diode junction. With the diode operating in the avalanche mode, the electron current across the junction is large enough that the shot noise follows a Gaussian voltage distribution. To verify this we have repetitively sampled the waveform of the noise using a wide-bandwidth waveform digitizer interfaced to a desktop computer and then determined the probability distribution of the voltage

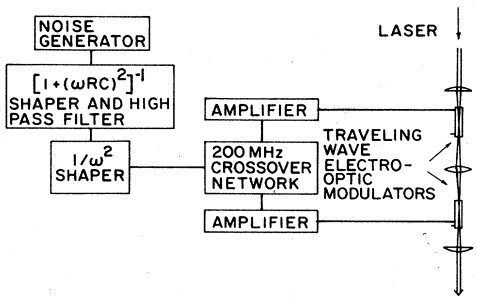

FIG. 3. Detailed diagram of the phase-modulation apparatus used for superposing high-frequency fluctuations onto the laser frequency.

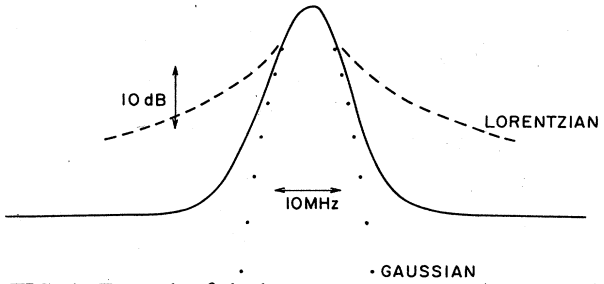

FIG. 4. Example of the laser power spectrum (superposed on the noise baseline of the spectrum analyzer) where $\beta/2\pi=1$ MHz and $b/2\pi=5.1$ MHz. The Lorentzian and Gaussian curves, which are shown for comparison, have been chosen to have the same FWHM (5.3 MHz) as the experimental curve. Note that the vertical scale is logarithmic.

$P(v_i)$. Figure 5 shows a typical plot of the distribution of the random voltage. The smooth line is a Gaussian profile whose width is determined by the root-mean-square voltage calculated from the data and whose height is determined by a least-squares-fitting routine. Also shown in Fig. 5 is a magnification ($\times 100$) of the noise distribution and the Gaussian curve, showing good agreement in the wings. The probability distribution is derived from 1200 digitized waveforms, each yielding 512 data points.

A more quantitative measure of the randomness of the noise sources is a comparison of the moments of the distribution with those of a true Gaussian function. The even moments of a Gaussian probability distribution are related by $\langle A^{2n}\rangle=[(2n)!/n!2^n]\langle A^2\rangle^n$, and the odd moments are zero.[12] Using the probability distribution of the noise $P(v_i)$ we calculated the actual moments up to tenth order for comparison with the Gaussian moments. The fractional deviation is shown in Table II for different noise sources. The deviation of the second-order moment is zero in all cases in Table II since the moments were normalized to this value. Uncertainties represent one standard deviation of the mean and are derived from the statistical scatter of the data. The last column in Table II shows similar data for a sine wave oscillating at 382 MHz. This serves as a test of the sampling method and the linearity of the digitizer. The tenth-order moment of the noise distribution can be seen to vary by typically

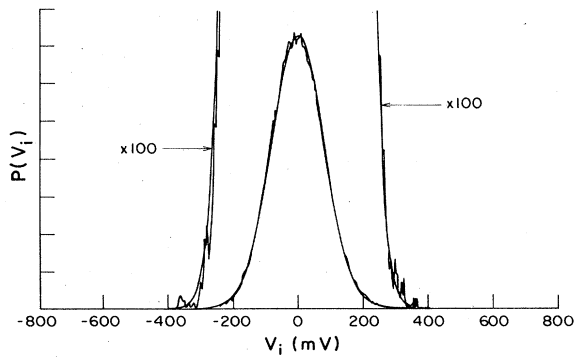

FIG. 5. Example of the distribution function of the random-voltage signal on which the laser modulation process is based. Exterior lines represent a magnification of the data ($\times 100$). Smooth curves show a Gaussian which best fits the data.

TABLE II. Examples of the fractional deviation of the even moments of the noise distribution from those required of a Gaussian process.

Moment	Low-frequency noise (%)	Low-frequency noise and amplifier (%)	Intermediate-frequency noise (%)	High-frequency noise (%)	Sine wave (%)
$\langle V^2 \rangle$	0±0.8	0±1.5	0± 1.7	0±1.0	0
$\langle V^4 \rangle$	0.2±2.1	0.1±2.9	−0.7± 3.4	−1.8±1.9	0.5
$\langle V^6 \rangle$	0.7±4.4	2.0±4.5	−1.5± 6.2	−4.8±3.0	1.3
$\langle V^8 \rangle$	2.1±8.2	6.4±6.3	−2.3±10.5	−8.1±4.6	2.4
$\langle V^{10} \rangle$	5.3±13.5	13.1±9.4	−3.7±16.5	−11.6±7.5	3.9

10% from the expected moment, and most of this deviation can be attributed to statistical error (for example, a 1% error in $\langle V^2 \rangle$ results in a 5% error in $\langle V^{10} \rangle$). We conclude therefore that the random voltages produced by the noise sources are very well described by a Gaussian distribution, and that distortion induced by subsequent amplification is minimal.

The technique used here for observing the two-photon Doppler-free absorption is similar to that described in previous reports[13] (see Fig. 6). The cw laser beam, tuned to one half the sodium $3^2S(F=2) \rightarrow 5^2S(F=2)$ transition, passes unfocused ($\sim$1-mm beam diameter) through a vapor cell containing atomic sodium. The laser beam is reflected back into the cell so that the sodium atoms may absorb one photon from each of the counterpropagating laser beams. Since the laser is linearly polarized, the sodium is also able to absorb both photons from either one of the laser beams, but only those atoms whose velocity "tunes" them into resonance with the laser can participate in this process. The absorption profile therefore consists of a narrow Doppler-free peak on top of a low-level Doppler-broadened background. The use of linearly polarized light restricts the interaction to $\Delta F=0$, $\Delta m_F=0$ transitions (see Fig. 7). The $3^2S(F=1) \rightarrow 5^2S(F=1)$ transition frequency differs by approximately 1600 MHz (Ref. 14) and does not interfere with the observations. The intermediate 3^2P state is detuned from a single-photon resonance with the laser by about 370 cm^{-1}, so that population of this state is negligible.

The absorption rate is measured by counting fluorescence photons at 330 nm corresponding to the second step in the $5S \rightarrow 4P \rightarrow 3S$ deexcitation of the sodium atoms (see Fig. 7). Approximately 43% of the atoms decay via this route;[15] the remainder decay by way of the $3P$ intermediate state. Spectral discrimination against scattered laser radiation favors this detection scheme. The detector is a photomultiplier, suitable for photon counting, which views the radiation at 330 nm through a narrow-band interference filter. The detection solid angle is approximately $4\pi/50$. The output of the photomultiplier was amplified ($\times 10$) and low-level pulses were eliminated by a discriminator to reduce the dark current count. The pulses (of approximately 20-nsec duration) were counted on a 45-MHz counter. Maximum count rates were typi-

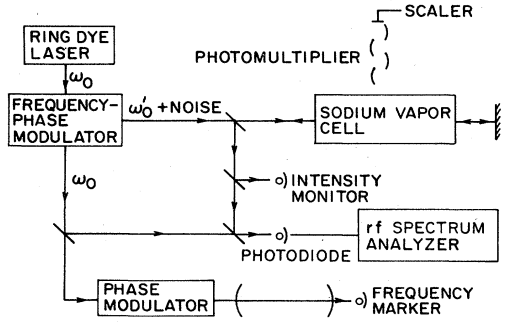

FIG. 6. Experimental setup. The block labeled frequency-phase modulator represents the hybrid modulation apparatus consisting of a series combination of the apparatus shown in Figs. 2 and 3. The modulated unfocused laser beam is directed into the sodium vapor cell and reflected back on itself in a manner typical of Doppler-free two-photon absorption experiments. The frequency marker provides an absolute calibration of the laser frequency scan, and the spectrum analyzer is part of a heterodyne detection scheme for monitoring the laser power spectrum.

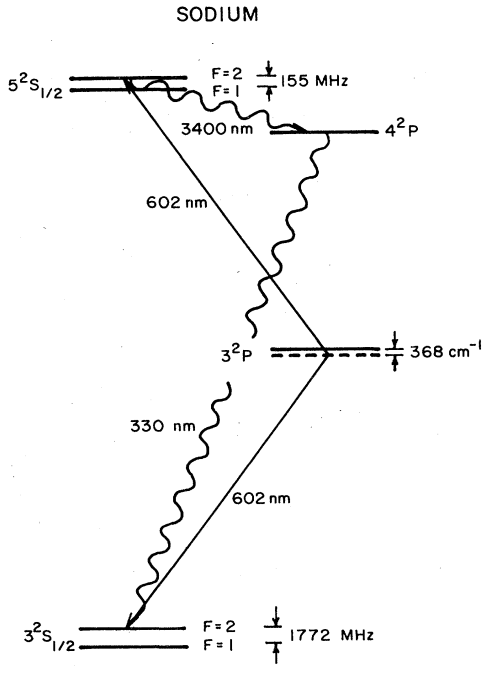

FIG. 7. Energy-level diagram of sodium showing the spectroscopic data relevant to this experiment.

cally 10 kHz, so that superposition errors were negligible. The temperature of the sodium cell was ~ 160°C, and the density of sodium atoms ($\sim 10^9$ atoms cm^{-3}) was controlled by the temperature of a cold finger on the cell.

The absorption profile was determined by stepping (256 steps) the laser frequency through the resonance and recording the fluorescence intensity as described above. Counting times for each step of the scan ranged from 50 to 300 msec and typically 200—500 photons per step were detected at the peak of the absorption profile. The frequency scan was controlled and the count rate recorded by a minicomputer. The intensity and the frequency of the laser were recorded at the same time the absorption profile was recorded. The frequency was monitored by passing a sample of the unmodulated laser beam through a Fabry-Perot interferometer (free spectral range=380 MHz) in a near-confocal arrangement. This provided transmission peaks at a frequency spacing of 35.7 MHz. For finer frequency discrimination, in the case of shorter laser scans, sidebands with a 10-MHz spacing were imposed on the laser using a traveling-wave electro-optic phase modulator. These frequency markers provided an absolute calibration on the width of the absorption peak. Figure 8 shows an example of the absorption spectrum and the Fabry-Perot transmission.

The power spectrum was recorded and checked typically two or three times during the time required for the measurements of a set of typically ten two-photon absorption spectra. To observe the laser bandwidth effects to the best advantage, it is necessary to minimize the spectral width of the transition due to all other broadening mechanisms. The natural lifetime of the $5S$ state in sodium is 80 nsec, resulting in a linewidth of 2 MHz. The observed linewidth in the absence of laser fluctuations was approximately 4 MHz. Collisional broadening due to the presence of a foreign gas in the vapor cell is the probable cause of the additional broadening. Transit-time broadening, due to the finite interaction time of the atom with the laser field as the atom travels through the laser beam, is estimated to be 500 kHz and may contribute minimally to the width as well. No evidence of this was observable, however, as the laser-beam diameter was varied.

Zeeman splitting is not observable because the Landé g factor of the initial $3S$ state is the same as that of the final $5S$ state. The ionization rate is calculated to be 200 Hz, using the ionization cross section of the $5S$ state as determined by Smith *et al.*[16] for radiation at 1.06 μm. The cross section at 602 nm is expected to be smaller than this measured value. Level shifts resulting from the interaction of the atom with the optical field (ac Stark shifts) are also minimal. The shift of the $3S$ state dominates that of the $5S$ state and can be calculated[17] to be approximately 1 Hz for the laser intensity of 7 W/cm^2 used in the experiment.

It is also important that the statistical properties of the laser beam not vary as the laser propagates through the absorption cell. No attenuation of the laser beam was observable. Estimates of the absorption based on the observed fluorescence and accounting for the solid angle subtended by the lens collecting the fluorescence radiation ($4\pi/50$), quantum efficiency of the detector ($\sim 26\%$), and the branching ratio of the radiation decay (0.43) indicate that the fractional decrease in the light intensity is $\sim 10^{-6}$.

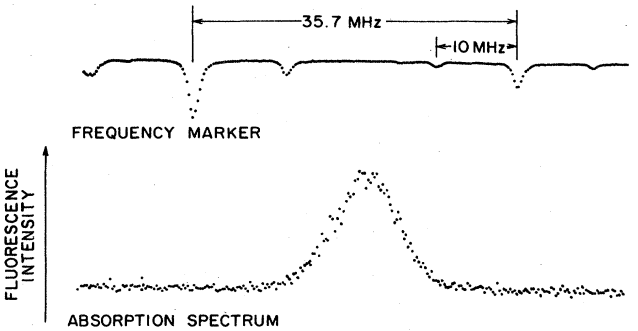

FIG. 8. Example of the absorption spectrum, and the frequency marker derived from the transmission of the unmodulated laser by a Fabry-Perot interferometer. The laser power spectrum with which these data were taken is shown in Fig. 4.

No evidence of saturation of the two-photon transition was observable. Estimates based on the observed fluorescence rate and a known dipole transition moment indicate that the laser intensity was more than 3 orders of magnitude less than that required for saturation.

IV. EXPERIMENTAL RESULTS

The widths of the two-photon absorption spectra obtained in the manner described were measured for many different laser power spectra. The spectral density of the fluctuations b, the correlation time of the fluctuations β^{-1}, and the delay time between the two fields τ_D were varied in order to determine the dependence of the absorption spectra on these parameters. The results are shown in Fig. 9 where the widths of the absorption spectra are plotted versus the widths of the laser power spectra.

The data points in Fig. 9 represent the average of the absorption width as measured from typically ten absorption spectra. The vertical error bars indicate a standard deviation of the mean of these measurements. The horizontal error bars indicate a 10% uncertainty in calibration of the rf spectrum analyzer used in determining the laser spectral width. In each figure, the solid line indicates the numerical calculation of the two-photon absorption width using Eqs. (4) and (6). The only parameter which was not controlled by the experimental geometry or the fluctuations apparatus was the absorption width of the transition when the frequency fluctuations were absent, i.e., when the laser had a narrow bandwidth. This value was measured to be approximately 4 MHz, as discussed in Sec. III.

In Figs. 9(a)—9(c), the laser power spectra are nearly Lorentzian in shape, since the correlation frequency $\beta/2\pi$ is 100 Mhz and the spectral density of the fluctuations $b/2\pi$ is at most 7 MHz. Recall that in the limit of a true Lorentzian line shape ($\beta \to \infty$), $b/2\pi$ corresponds to the HWHM of the power spectrum. Figures 9(a)—9(c) differ from each other in the delay time imposed between the incident and retroreflected laser beam.

As the distance between the reflector and the sodium

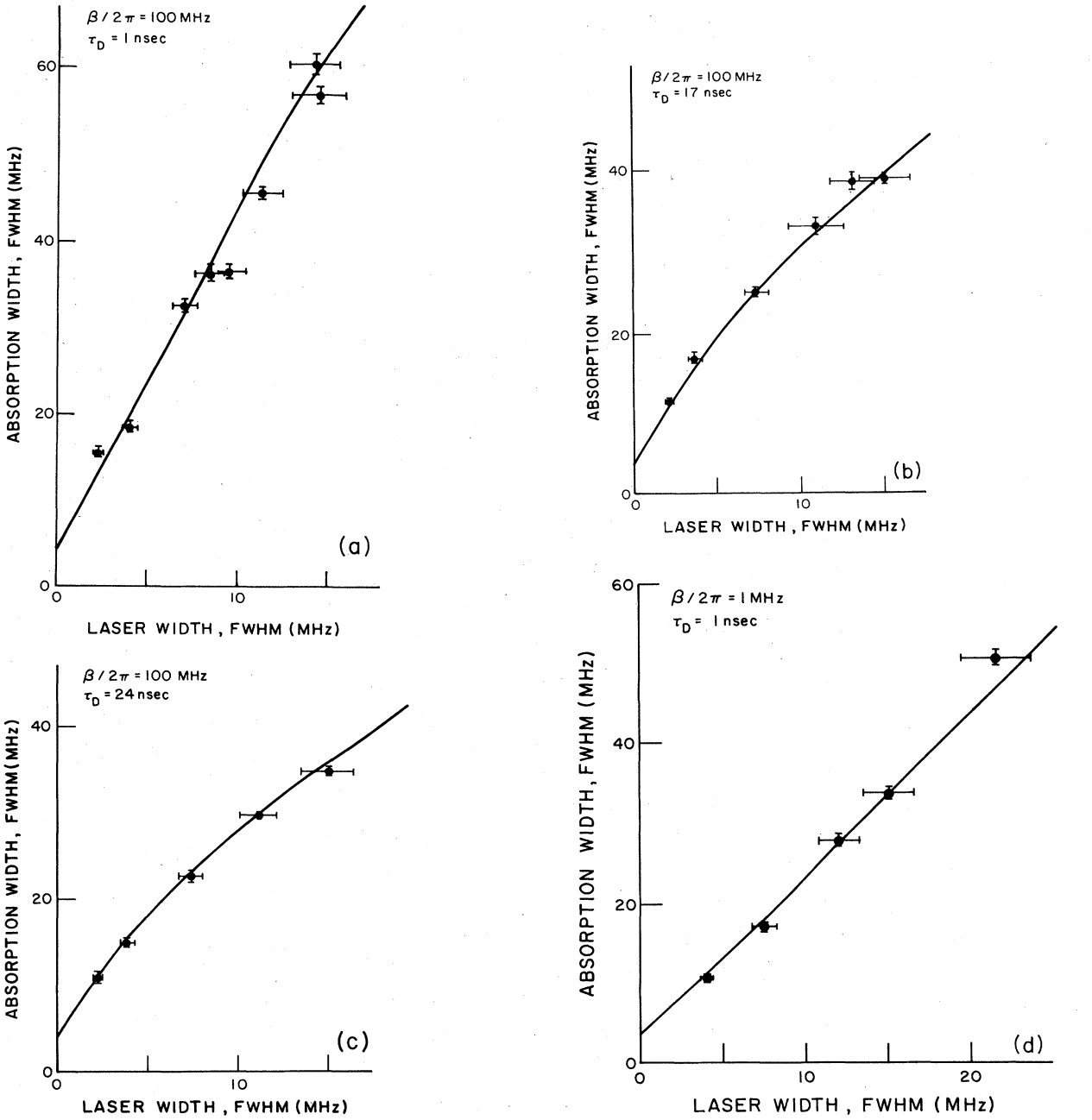

FIG. 9. Width of the two-photon absorption peak vs the width of the laser for various values of the delay time τ_D and correlation frequency of the frequency fluctuations β. Figures (a)—(c) represent a nearly Lorentzian laser power spectrum, with $\beta/2\pi=100$ MHz, and (d) a nearly Gaussian laser power spectrum, with $\beta/2\pi=1$ MHz. The delay time for (a)—(d) are 1, 17, 24, and 1 nsec, respectively.

cell is increased, the degree of correlation between the two fields with which the atom interacts is decreased. The time necessary for decorrelation for the laser field is estimated to be $\sim 1/2b=16$ nsec for a 10-MHz FWHM Lorentzian beam. Since the widths of the laser power spectra range to 15 MHz (FWHM) and the maximum delay time is 24 nsec, the effect of the field decorrelation is not unexpected. In Fig. 9(a), the data points for small bandwidths are easily fitted by a line of slope 4, in agreement with Mollow's calculations. The deviation of the line from a straight line for bandwidths greater than 10 MHz is due to the finite correlation time of the fluctuations (i.e., the laser power spectrum is becoming less Lorentzian). For a purely Lorentzian laser line, the delay time required for decorrelation of the laser beams is related inversely to the laser bandwidth (see Table I) and this short delay time is not expected to be significant until the laser bandwidth is increased to approximately $2/2\pi$

$\times 1/2\tau_D = 160$ MHz (FWHM).

In Figs. 9(b) and 9(c), the delay time has been increased to 17 and 24 nsec, respectively. This is accomplished by increasing the distance between the sodium cell and the reflector from 15 cm to 2.55 and 3.65 m, respectively. The solid line is calculated numerically as described previously, and the effect of the nonzero delay time is apparent.

Results for nearly Gaussian laser power spectra are shown in Fig. 9(d). The correlation frequency of the fluctuations in this case is $\beta/2\pi = 1$ MHz, and the laser bandwidth ranges from 4 to 20 MHz. The solid line representing the numerical calculation has a slope of nearly 2, as expected for the Gaussian line shape. No effect of decorrelation due to the delay time is expected in this case for experimental arrangements possible in the laboratory, as a round-trip delay length of $2\pi c/\beta = 1.9$ km is required before this effect is observable.

The bandwidth of the laser is also observed to affect the height of the absorption spectrum, corresponding to the transition rate when the laser is tuned to exact resonance with the transition. The height of the absorption curve, normalized to the height of the absorption spectra in the absence of fluctuations, agrees well with values determined from numerical evaluation of Eqs. (4) and (6).

V. CONCLUSION

The results presented in this paper indicate the importance of field statistics in nonlinear optical processes. In this case, pronounced differences in the two-photon absorption process from a phase-diffusing laser field can be seen when field correlations are varied. For example, the absorption width is shown to be four times the laser width in the case of a nearly Lorentzian laser power spectrum when the incident and counter propagating laser beams are completely correlated, in agreement with time-dependent perturbation-theory results of Mollow.[3] A delay of the counter propagating laser beam results in a decorrelation of the two fields and a subsequent decrease in the width of the absorption spectrum. For complete decorrelation, or using independently generated laser fields, the absorption width is expected to be twice the laser width.

Similar results are presented for a nearly Gaussian laser power spectrum. The absorption width was observed to be twice the laser width as expected. Although decorrelation of the Gaussian field through the introduction of a time delay is not practical because of the large distances required, a further decrease in the width of the absorption profile would be expected.

ACKNOWLEDGMENT

This work was supported by the U.S. Department of Energy, Office of Basic Energy Sciences. We wish to acknowledge very helpful conversations with Gernot Alber, particularly concerning the generalized form of the correlation function [Eq. (6)].

*Present address: School of Electrical Engineering, Purdue University, West Lafayette, IN 47907.

†Quantum Physics Division, National Bureau of Standards, Boulder, CO 80309.

[1]D. S. Elliott, M. W. Hamilton, K. Arnett, and S. J. Smith, Phys. Rev. Lett. **53**, 439 (1984).

[2]D. S. Elliott, in *Multiphoton Processes,* 3rd International Conference, Iraklion, Crete, Greece, edited by P. Lambropoulos and S. J. Smith (Springer, Berlin, 1984), p. 76.

[3]B. R. Mollow, Phys. Rev. **175**, 1555 (1968).

[4]G. S. Agarwal, Phys. Rev. A **1**, 1445 (1970).

[5]G. H. Alber and P. Zoller, J. Phys. B **13**, 4567 (1980).

[6]P. Zoller and P. Lambropoulos, J. Phys. B **13**, 69 (1980).

[7]J. J. Yeh and J. H. Eberly, Phys. Rev. A **24**, 888 (1981).

[8]D. S. Elliott, R. Roy, and S. J. Smith, Phys. Rev. A **26**, 12 (1982).

[9]D. S. Elliott, R. Roy, and S. J. Smith, in *Spectral Line Shapes, Volume 2,* edited by K. Burnett (de Gruyter, Berlin, 1983), p. 989.

[10]D. Middleton, Philos. Mag. **42**, 689 (1951).

[11]M. C. Wang and G. E. Uhlenbeck, Rev. Mod. Phys. **17**, 323 (1945).

[12]For example, A. Papoulis, *Probability, Random Variables and Stochastic Processes* (McGraw-Hill, New York, 1965), p. 147.

[13]See, for example, D. Pritchard, J. Apt, and T. W. Ducas, Phys. Rev. Lett. **32**, 641 (1974); F. Biraben, B. Cagnac, and G. Grynberg, *ibid.* **32**, 643 (1974); M. D. Levenson and N. Bloembergen, *ibid.* **32**, 645 (1974).

[14]For example, M. M. Salour, Ann. Phys. **111**, 364 (1978).

[15]A. Lindgård and S. E. Nielsen, At. Nucl. Data Tables **19**, 533 (1977).

[16]A. V. Smith, J. E. M. Goldsmith, D. E. Nitz, and S. J. Smith, Phys. Rev. A **22**, 577 (1980).

[17]S. N. Dixit and P. Lambropoulos, Phys. Rev. A **27**, 861 (1983).